Magnetic Field Analysis of
Spherical Actuators with Iron Stator

Liang Yan, I-Ming Chen, Chee Kian Lim
School of Mechanical and Aerospace
Engineering, Nanyang Technological
University, Singapore 639798
yanliang@ntu.edu.sg, michen@ntu.edu.sg

Guilin Yang, Wei Lin
Mechatronics Group, Singapore
Institute of Manufacturing
Technology, Singapore 638075
glyang@SIMTech.a-star.edu.sg

Kok-Meng Lee, *Fellow, IEEE*
George W. Woodruff School of
Mechanical Engineering, Georgia
Institute of Technology, USA 30332
kokmeng.lee@me.gatech.edu

Abstract—This paper presents a ball-joint-like three-degree-of-freedom (3-DOF) permanent magnet (PM) spherical actuator which features a ball-shaped rotor with multiple PM poles and a spherical iron stator with air-core coils. The magnetic field of the PM-pole rotor of this PM spherical actuator is formulated analytically. Simulation result of the magnetic field variation is then presented. In addition, the effect of the stator iron on the magnetic field is evaluated, which is very useful for design of PM spherical actuators.

Index Terms—spherical actuator, magnetic field, iron stator

I. INTRODUCTION

Compared with conventional three-degree-of-freedom (3-DOF) spherical motion mechanism by using several single-axis actuators connected in parallel or in series, a spherical actuator that can generate multi-DOF rotational motion in one joint has the advantages of compact structure, fast response and singularity free in workspace. Williams and Laithwaite [1] [2] have designed the first 2-DOF spherical induction motor. The magnetic field generated by the stator windings induces a current on the rotor surface, and causes the rotor to incline. Davey *et al.* [3] derived the torque model of this induction motor by integrating the Maxwell stress moment over the spherical rotor surface and proposed its use as a robot wrist [4]. The mechanical complexity and the inherent poor servo characteristics of the spherical induction motor led Lee *et al.* [5] to develop a 3-DOF spherical stepper based on the principle of variable-reluctance. The torque output of a variable-reluctance spherical motor (VRSM) depends on the current inputs as well as the magnetic reluctance at the air-gaps between the rotor and the stator poles [6]. In the past decade, several variations of spherical motors with a structure similar to [5] have been studied. Wang *et al.* [7]–[10] have developed spherical actuators achieving 2/3-DOF motions. The rotor is a completely magnetized ball. Coils are uniformly mounted on the stator. Chirikjian *et al.* [11] have made a spherical stepper with a permanent magnet (PM) pole rotor and a stator with an array of coils. Difference in the symmetric layout of the rotor poles and the stator poles allows stepping motion in three orientations. Kahlen *et al.* [12] developed a spherical motor consisting of a rotor sphere with 112 PM poles and an outer stator with 96 stator windings. More recently, Lee *et al.* [13] [14] have developed a spherical wheel motor that offers
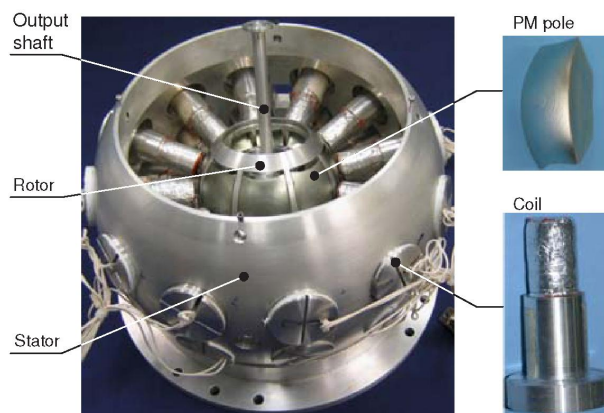

Fig. 1.   Prototype of spherical actuator

a means to control the orientation of its rotating shaft in an open-loop fashion.

In our previous study [15] [16], a research prototype of PM spherical actuator has been developed as shown in Fig. 1. The key feature of this spherical actuator is its flexible structure, i.e., the relationship between the torque output and structure parameters can be described so that optimum values of parameters can be selected to achieve high torque output [17]. Furthermore, more PM and coil poles are allowed to incorporate, and thus to increase the working range as well as motion resolution of the actuator. In this prototype, the stator is made from aluminum for preliminary study. As ferromagnetic materials such as soft iron may reduce the magnetic energy loss and increase the actuator torque, the objective of this paper is to derive mathematic model of the three-dimensional (3D) magnetic field of PM spherical actuators with a laminated-soft-iron stator, and to analyze the effect of stator iron on the magnetic field distribution.

II. WORKING PRINCIPLE

The working principle of the proposed spherical actuator is illustrated in Fig. 2. Rare earth PM poles (NdFeB) mounted along the rotor equator can produce high flux density. The air-core coils are assembled on the stator which can simplify the torque model of the spherical actuator in a linear fashion. By

activating pairs of coils in two longitudinal directions, the rotor can tilt in two orthogonal directions as shown in Fig. 2(a) and 2(b). Energizing all circumferential coils, the rotor can spin about its own axis (Fig. 2(c)). Therefore, by varying the input currents of coils, any desirable 3-DOF spherical motion within the workspace can be achieved.
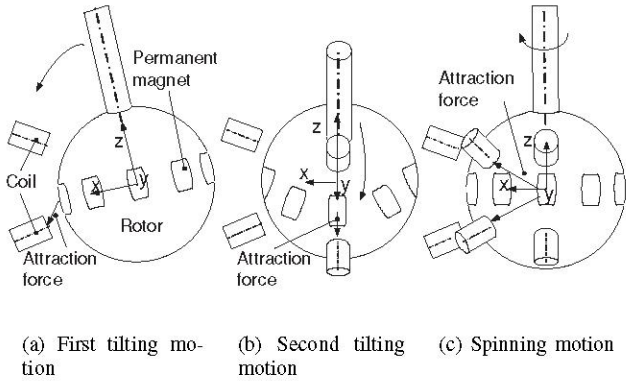

(a) First tilting motion   (b) Second tilting motion   (c) Spinning motion

Fig. 2. 3-DOF motion of spherical actuator

III. FORMULATION OF MAGNETIC FIELD

The torque output of PM spherical actuator is generated by the interaction between the magnetic field of PM rotor and the current in coils. Therefore, analysis of PM rotor's magnetic field is a precondition of torque modeling of spherical actuator which in turn is significant for actuator control. The challenge of magnetic field formulation for spherical actuators is that the magnetic flux density has three components, and each of those components varies in the 3D space. In this research, Laplace's equation is employed to solve the magnetic scalar potential of the PM rotor, and thus to obtain the formulation of magnetic field distribution surrounding the rotor.

A. Assumptions

Assumptions that are useful for the formulation of magnetic field are listed as follows.

- The magnetic permeability of air space is the same as that of free space.
- The magnetic permeability of stator iron is much greater than that of air space.
- PMs are assumed to be ideal with field relationship described by the linear second quadrant of a PM demagnetization curve.

B. Characterization of Rotor Space

In formulating the magnetic field of the rotor, we use a generic spherical rotor model as shown in Figure 3 for discussion. The PM poles are evenly spaced (with alternate polarities) around the rotor equator, each of which has the shape of a dihedral cone defined in terms of four parameters: longitudinal angle α, latitudinal angle β, outer and inner radii, R_r and R_b. With such an arrangement on PM pole, the study of rotor magnetic field can be divided into three parts.

1) Air Space outside the Rotor (Region 1): The air gap is a linear homogeneous media with the absence of magnetization, which can be characterized by a constitutive relation

$$\mathbf{B}_1 = \mu_0 \mathbf{H}_1, \tag{1}$$

where the subscript "1" denotes Region 1; $\mathbf{B}$ and $\mathbf{H}$ are the magnetic flux density and field intensity; and μ_0 is permeability of free space with a value of $4\pi \times 10^{-7}$ H/m.

2) Within the Dihedral PM Rotor Poles (Region 2): In this study, PMs are assumed to be ideal with field relationship described by the linear second quadrant of a PM demagnetization curve. Therefore, the magnetic property of PM can be characterized by

$$\mathbf{B}_2 = \mu_0 \mu_m \mathbf{H}_2 + \mu_0 \mathbf{M}_0, \tag{2}$$

where μ_m is the dimensionless relative recoil permeability of PM (typical value ranging between 1.05 and 1.20); $\mathbf{M}_0 = \mathbf{B}_{rem}/\mu_0$ is the residual magnetization vector in A/m; and $\mathbf{B}_{rem}$ is defined as the remanence in Tesla. In spherical coordinates, the residual magnetization vector of the pth PM can be expressed as

$$\mathbf{M}_0 = \begin{bmatrix} M_{0,r} \\ M_{0,\theta} \\ M_{0,\phi} \end{bmatrix} = (-1)^{p-1} |\mathbf{M}_0| \begin{bmatrix} \cos(\phi - \alpha_p) \sin\theta \\ \cos(\phi - \alpha_p) \cos\theta \\ -\sin(\phi - \alpha_p) \end{bmatrix}, \tag{3}$$

where $\alpha_p = \alpha/2 + 2\pi(p-1)/P$, $p = 1, 2, ..., P$. P is the total number of PM poles. In this study, let $P = 8$. Note that these equations are only valid within the range of

$$0 < \phi - \frac{2\pi(p-1)}{P} < \alpha, \quad \frac{\pi}{2} - \frac{\beta}{2} < \theta < \frac{\pi}{2} + \frac{\beta}{2}.$$

For the non-magnetized space in between poles on the rotor, the residual magnetization is equal to zero.

3) Rotor Core Made of Ferromagnetic Material (Region 3): The magnetic property of ferromagnetic material such as soft iron can be characterized as

$$\mathbf{B}_3 = \mu_0 \mu_r \mathbf{H}_3, \tag{4}$$

where μ_r is relative permeability of the ferromagnetic core.

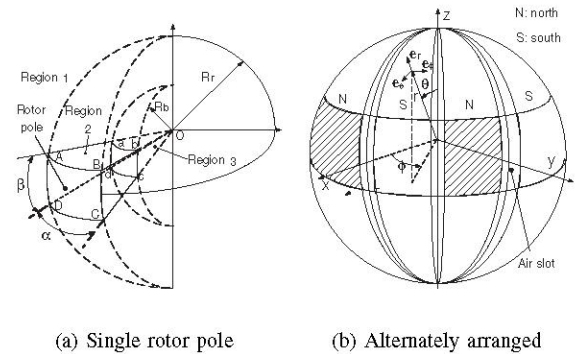(a) Single rotor pole   (b) Alternately arranged

Fig. 3. Arrangement of rotor poles

C. Governing Equations

For an irrotational magnetic field,

$$\nabla \times \mathbf{H} = 0, \qquad \nabla \cdot \mathbf{B} = 0, \qquad (5)$$

where $\mathbf{H}$ is curl free and can be expressed in terms of a scalar potential function Φ based on Helmholtz's theorem:

$$\mathbf{H} = -\nabla\Phi. \qquad (6)$$

In spherical coordinates,

$$\begin{aligned}
\mathbf{H} &= H_r\mathbf{e}_r + H_\theta\mathbf{e}_\theta + H_\phi\mathbf{e}_\phi \\
&= \left[-\frac{\partial\Phi}{\partial r}, \; -\frac{1}{r}\frac{\partial\Phi}{\partial\theta}, \; -\frac{1}{r\sin\theta}\frac{\partial\Phi}{\partial\phi}\right]^T,
\end{aligned} \qquad (7)$$

where $\mathbf{e}_r$, $\mathbf{e}_\theta$ and $\mathbf{e}_\phi$ are respective unit vectors, H_r, H_θ and H_ϕ are components of magnetic field intensity.

For Regions 1 and 3, the scalar potentials are governed by the Laplace's equations:

$$\nabla^2\Phi_1 = 0, \qquad \nabla^2\Phi_3 = 0. \qquad (8)$$

The scalar potential Φ_2 within Region 2 is expressed as

$$\nabla^2\Phi_2 = \nabla \cdot \mathbf{M}_0/\mu_m, \qquad (9)$$

which is in the form of Poisson's equation. With a symmetric arrangement of rotor poles, the divergence of the residual magnetization vector is equal to zero. Thus, the Poisson's equation can be reduced to Laplace's equation, $\nabla^2\Phi_2 = 0$.

D. General Solution to Laplace's Equations

The Laplace's equation can be written in spherical coordinates as:

$$\frac{1}{r^2}\left[\frac{\partial}{\partial r}(r^2\Phi_i) + \frac{1}{\sin\theta}\frac{\partial}{\partial\theta}(\sin\theta\frac{\partial\Phi_i}{\partial\theta}) + \frac{1}{\sin^2\theta}\frac{\partial\Phi_i}{\partial\phi}\right] = 0, \qquad (10)$$

where i (= 1, 2 and 3) denotes the region of concern. Based on the separation of variables, the general solution to the Laplace's equations characterizing all three regions has the following form [18]

$$\Phi_i = \sum_{n=0}^{\infty}\sum_{m=-n}^{n}(\kappa_{n,i}^m r^n + \xi_{n,i}^m r^{-(n+1)})Y_n^m(\theta,\phi), \qquad (11)$$

where $\kappa_{n,i}^m$ and $\xi_{n,i}^m$ are constants to be determined by the boundary conditions. The angular part of the solutions to the Laplace's equation, Y_n^m, is a complex valued spherical harmonic function defined by

$$Y_n^m(\theta,\phi) = S_n^m P_n^m(\cos\theta)e^{im\phi},$$

where $S_n^m = \sqrt{\dfrac{2n+1}{4\pi}\dfrac{(n-m)!}{(n+m)!}}$; $P_n^m(\cos\theta)$ is associated Legendre functions; n, m are integers with the condition $-n \le m \le n$.
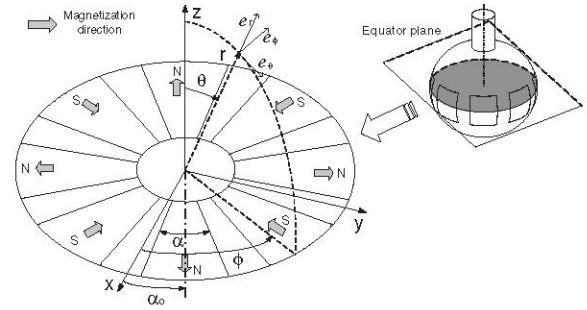
E. Spherical Harmonic Expansion of M_{0r}

To utilize the continuity on the boundary conditions between two medians, the radial component of residual magnetization vector needs to be expanded in spherical harmonics. Let M_0 be the magnitude of the residual magnetization vector $\mathbf{M}_0$. With reference to Fig. 4 that illustrates the poles placement on the equatorial plane of the rotor, the constituents M_{0r}, $M_{0\theta}$ and $M_{0\phi}$ of $\mathbf{M}_0$ in the directions $\mathbf{e}_r$, $\mathbf{e}_\theta$ and $\mathbf{e}_\phi$ are computed as

$$M_{0r} = (-1)^{p-1}M_0\cos[\phi - \alpha_0 - \frac{2\pi}{P}(p-1)]\sin\theta, \quad (12)$$

$$M_{0\theta} = (-1)^{p-1}M_0\cos[\phi - \alpha_0 - \frac{2\pi}{P}(p-1)]\cos\theta, \quad (13)$$

$$M_{0\phi} = (-1)^p \; M_0\sin[\phi - \alpha_0 - \frac{2\pi}{P}(p-1)], \qquad (14)$$

where $p = 1, 2, ..., P$. P is the total number of PM poles. In this study, $P = 8$, and α_0 is the PM pole angle at the center line in ϕ-direction. Note that these equations are only valid within the range of

$$\frac{\pi}{4}(p-1) + \alpha_0 - \frac{\alpha}{2} < \quad \phi \quad < \frac{\pi}{4}(p-1) + \alpha_0 + \frac{\alpha}{2}, \quad (15)$$

$$\frac{\pi}{2} - \frac{\beta}{2} < \quad \theta \quad < \frac{\pi}{2} + \frac{\beta}{2}, \qquad (16)$$

in the PM pole (Region 2). For the rest non-magnetized regions in the rotor, the residual magnetization is equal to zero.

When applying boundary conditions to solve the unknowns in the general solution of scaler potential, only the radial component of residual magnetization vector M_{0r} will be used to express the flux density continuity between regions. Components $M_{0\theta}$ and $M_{0\phi}$ do not exist in any boundary condition. The radial component can be expressed as an expansion of spherical harmonic functions $Y_n^m(\theta,\phi)$ as [19]:

$$M_{0r}^s(\theta,\phi) = \sum_{n=0}^{\infty}\sum_{m=-n}^{n}C_{nm}Y_n^m(\theta,\phi), \qquad (17)$$

where C_{nm} are coefficients determined from

$$C_{nm} = \int_0^\pi\int_0^{2\pi}M_{0r}(\theta,\phi)Y_n^{m*}(\theta,\phi)\sin\theta d\theta d\phi, \qquad (18)$$

and $Y_n^{m*}(\theta,\phi)$ denotes the complex conjugate of $Y_n^m(\theta,\phi)$. Substituting Eqn. (12) into Eqn. (18) gives the coefficients

$$C_{nm} = M_0\int_0^{2\pi}f(\phi)e^{-im\phi}d\phi\int_0^\pi S_n^m[P_n^m(\cos\theta)]\sin^2\theta d\theta, \quad (19)$$

1052

where

$$f(\phi) = (-1)^{p-1}\cos[\phi - \alpha_0 - \frac{\pi}{4}(p-1)], \quad p = 1, 2, ..., 8. \quad (20)$$

It is found that $C_{nm} \neq 0$ if and only if $m = \pm 4, \pm 12, \pm 20, ...$ Thus, fundamental terms of the spherical harmonic functions can be taken at $n = 4$ and $m = \pm 4$. For simplicity, only these terms are used for the derivation of magnetic field. Denote

$$a \pm bi \equiv \int_0^{2\pi} f(\phi)e^{-im\phi}d\phi \quad (m = 4 \text{ and } m = -4), \quad (21)$$

$$c/\sqrt{\pi} \equiv \int_0^{\pi} S_n^m \sin^2\theta[P_n^m(\cos\theta)]d\theta, \quad (22)$$

where a, b and c are real numbers. As M_{0r} is available within the range defined by Eqns. (15) and (16), integrals in Eqns. (21) and (22) are also constrained by the same range. Out of this range, the integrals are equal to zero. It can be verified that the results of Eqn. (22) for $m = 4$ and $m = -4$ are the same. Consequently, the coefficients $C_{4,4}$ and $C_{4,-4}$ can be obtained based on Eqn. (19) as

$$C_{4,4} = M_0 \frac{1}{\sqrt{\pi}}(a + bi)c, \quad C_{4,-4} = M_0 \frac{1}{\sqrt{\pi}}(a - bi)c, \quad (23)$$

where $C_{4,-4}$ is the complex conjugate of $C_{4,4}$. Therefore, the radial component M_{0r} of residual magnetization vector can be expressed in terms of spherical harmonics as

$$M_{0r}^s(\theta, \phi) = C_{4,-4}Y_4^{-4}(\theta, \phi) + C_{4,4}Y_4^4(\theta, \phi), \quad (24)$$

where $Y_4^{-4} = 3/16\sqrt{35/2\pi}\sin^4\theta e^{-4i\phi}$ and $Y_4^4 = 3/16\sqrt{35/2\pi}\sin^4\theta e^{4i\phi}$.

F. Boundary Conditions

The particular solutions that characterize the magnetic scalar potentials of three regions require the specification of the source term and the six unknowns, $\kappa_{n,i}^m$ and $\xi_{n,i}^m$ where $i = 1$, 2 and 3. These unknowns can be solved from the following boundary conditions (BC):

1) Boundary Condition A ($B_{1,\theta}|_{r=Rs} = 0$ and $B_{1,\phi}|_{r=Rs} = 0$): When magnetic flux goes from air space to ferromagnetic material with very high permeability, the direction of the magnetic flux is always normal to the interface between these two materials [20]. As soft iron is employed for the stator, the magnetic flux generated by the PM rotor is normal to the stator inner surface in Region 1. In other words, the tangential components of the magnetic flux $B_{1,\theta}|_{r=R_s}$ and $B_{1,\phi}|_{r=R_s}$ are equal to zero at the stator inner surface, where R_s is the inner stator radius. It can be obtained that

$$\xi_{n,1}^m = -\kappa_{n,1}^m R_s^{2n+1}. \quad (25)$$

2) Boundary Condition B ($B_{1,r}|_{r=R_r} = B_{2,r}|_{r=R_r}$): According to the conservation law of magnetic flux [21], on the interface of two neighboring medium with different permeability, the normal components of the flux density in both medium are equal to each other. Therefore, for Region 1 (air) and Region 2 (PM), there is boundary condition of $B_{1,r}|_{r=R_r} = B_{2,r}|_{r=R_r}$, where R_r is the radius of the rotor

that defines the spherical boundary between these two regions. Projecting all terms of Eqn. (2) into the r-direction gives

$$B_{2,r} = \mu_0\mu_m H_{2,r} + \mu_0 M_{0,r}. \quad (26)$$

From Eqns. (7), (17) and (26), it can be obtained that

$$-(n\kappa_{n,1}^m R_r^{2n+1} - (n+1)\xi_{n,1}^m)$$
$$= -\mu_m[n\kappa_{n,2}^m R_r^{2n+1} - (n+1)\xi_{n,2}^m] + C_{nm}R_r^{n+2}. \quad (27)$$

3) Boundary Condition C ($H_{1,\phi}|_{r=R_r} = H_{2,\phi}|_{r=R_r}$ and $H_{1,\theta}|_{r=R_r} = H_{2,\theta}|_{r=R_r}$): According to Ampere's circuital law [21], the tangential components of magnetic intensity on both sides are equal on the interface of two medium with different permeability. For the spherical actuator, there are two components H_θ and H_ϕ of the magnetic field intensity which are tangent to the rotor surface between Region 1 (air) and Region 2 (PM). Therefore, $H_{1,\phi}|_{r=R_r} = H_{2,\phi}|_{r=R_r}$ and $H_{1,\theta}|_{r=R_r} = H_{2,\theta}|_{r=R_r}$, where $r = R_r$ defines the boundary surface between Region 1 (air) and 2 (PM). From Eqns. (7), (11) and BC-C, the following result can be obtained

$$\kappa_{n,1}^m R_r^{2n+1} + \xi_{n,1}^m = \kappa_{n,2}^m R_r^{2n+1} + \xi_{n,2}^m. \quad (28)$$

4) Finite Boundary Condition D ($B_{3,r}|_{r=0} \neq \infty$, $B_{3,\theta}|_{r=0} \neq \infty$ and $B_{3,\phi}|_{r=0} \neq \infty$): This boundary condition comes from the fact that it is impossible to achieve an infinite value of flux density. According to Eqns. (7) and (11), the boundary condition, $B_{3,r}|_{r=0} \neq \infty$, can give $\xi_{n,3}^m = 0$. It can be verified that $B_{3,\theta}|_{r=0} \neq \infty$ and $B_{3,\phi}|_{r=0} \neq \infty$ yield the same result.

5) Boundary Condition E ($B_{2,r}|_{r=R_b} = B_{3,r}|_{r=R_b}$): This boundary condition is similar to BC-B. Following the same development, BC-E gives the following result

$$\mu_r n\kappa_{n,3}^m R_b^{2n+1} = \mu_m[n\kappa_{n,2}^m R_b^{2n+1} - (n+1)\xi_{n,2}^m] - C_{nm}R_b^{n+2} \quad (29)$$

6) Boundary Condition F ($H_{2,\phi}|_{r=R_b} = H_{3,\phi}|_{r=R_b}$ and $H_{2,\theta}|_{r=R_b} = H_{3,\theta}|_{r=R_b}$): Following the same procedure of BC-C, $H_{2,\phi}|_{r=R_b} = H_{3,\phi}|_{r=R_b}$ can lead to

$$\kappa_{n,3}^m R_b^{2n+1} = \kappa_{n,2}^m R_b^{2n+1} + \xi_{n,2}^m. \quad (30)$$

$H_{2,\theta}|_{r=R_b} = H_{3,\theta}|_{r=R_b}$ also yields the same result.

G. Solution of Magnetic Flux Density

1) Solution of Unknowns in Scalar Potential: So far, the values or relationships of coefficients $\xi_{n,1}^m$, $\xi_{n,2}^m$, $\xi_{n,3}^m$, $\kappa_{n,1}^m$, $\kappa_{n,2}^m$ and $\kappa_{n,3}^m$ have been derived from boundary conditions. Specifically, BC-D produces the result of $\xi_{n,3}^m = 0$, and BC-A, BC-B, BC-C, BC-E and BC-F lead to Eqns. (25), (27), (28), (29) and (30) respectively. According to Lorentz force law, only the magnetic field in Region 1 (air) generates actuator torque. Therefore, solutions of $\xi_{n,1}^m$ and $\kappa_{n,1}^m$ are important for solving magnetic field distribution ($\kappa_{n1}^m = 0$). By taking advantage of Eqns. (25), (27), (28), (29) and (30), the following results can be achieved

$$\kappa_{n,1}^m = O_{n,5}C_{nm}. \quad (31)$$

$$\xi_{n,1}^m = O_{n,6}C_{nm}. \quad (32)$$

where

$$O_{n,6} = -(O_{n,3}/O_{n,4}R_r^{2n+1} - O_{n,2}/O_{n,1})/(R_r^{2n+1} - R_s^{2n+1})R_s^{2n+1},$$
$$O_{n,5} = (O_{n,3}/O_{n,4}R_r^{2n+1} - O_{n,2}/O_{n,1})/(R_r^{2n+1} - R_s^{2n+1}),$$
$$O_{n,4} = [(\mu_r - \mu_m)nR_b^{2n+1}],$$
$$O_{n,3} = [\mu_r n + \mu_m(n+1)]O_{n,2}/O_{n,1} - R_b^{n+2}$$
$$O_{n,2} = R_r^{n+2}(R_r^{2n+1} - R_s^{2n+1})(\mu_r - \mu_m)nR_b^{2n+1} - R_b^{n+2}R_r^{n+2}$$
$$\{nR_r^{2n+1}(1-\mu_m) + (n+1+\mu_m n)R_s^{2n+1}\},$$
$$O_{n,1} = \{[n+\mu_m(n+1)]R_r^{2n+1} + [(n+1) - \mu_m(n+1)]R_s^{2n+1}\}$$
$$(\mu_r - \mu_m)nR_b^{2n+1} - R_r^{2n+1}\{nR_r^{2n+1}(1-\mu_m) +$$
$$(n+1+\mu_m n)R_s^{2n+1}\}[\mu_r n + \mu_m(n+1)].$$

2) Scalar Potential and Magnetic Flux Density: Substituting κ_{nI}^m and ξ_{nI}^m into Eqn. (10) and discarding the high-order harmonic terms give

$$\Phi_1 = [\kappa_{4,1}^{-4}r^4 + \xi_{4,1}^{-4}r^{-5}][Y_4^{-4}(\theta,\phi)] + [\kappa_{4,1}^4 r^4 + \xi_{4,1}^4 r^{-5}][Y_4^4(\theta,\phi)]$$
$$= [O_{4,5}r^4 + O_{4,6}r^{-5}]\{C_{4,-4}[Y_4^{-4}(\theta,\phi)] + C_{4,4}[Y_4^4(\theta,\phi)]\}. (33)$$

Because $C_{4,4} = M_0\frac{1}{\sqrt{\pi}}(a+bi)c$ and $C_{4,-4} = M_0\frac{1}{\sqrt{\pi}}(a-bi)c$, it can be obtained that

$$\Phi_1 = \frac{3}{8}\sqrt{\frac{35}{2\pi}}\frac{cM_0}{\sqrt{\pi}}[O_{4,5}r^4 + O_{4,6}r^{-5}]\sin^4\theta(a\cos4\phi - b\sin4\phi). (34)$$

Therefore, three components of the magnetic flux density are calculated as (To simplify the equation, let $\alpha_0 = 0$.)

$$B_{1,r} = \frac{3}{8}\sqrt{\frac{35}{2\pi}}\frac{ac\mu_0 M_0}{\sqrt{\pi}}[5O_{4,6}r^{-6} - 4O_{4,5}r^3]\sin^4\theta\cos4\phi \quad (35)$$

$$B_{1,\theta} = -\frac{3}{2}\sqrt{\frac{35}{2\pi}}\frac{ac\mu_0 M_0}{\sqrt{\pi}}[O_{4,5}r^3 + O_{4,6}r^{-6}]\sin^3\theta\cos\theta\cos4\phi \quad (36)$$

$$B_{1,\phi} = \frac{3}{2}\sqrt{\frac{35}{2\pi}}\frac{ac\mu_0 M_0}{\sqrt{\pi}}[O_{4,5}r^3 + O_{4,6}r^{-6}]\sin^3\theta\sin4\phi \quad (37)$$

IV. SIMULATION AND ANALYSIS

A. Simulation Result

Let $\mathbf{B}_{rem} = 1T$, $R_b = 15mm$, $R_r = 45mm$ and $R_s = 80mm$. The distribution of three magnetic field components with respect to θ and ϕ is presented in Fig. 5 ($r = 46mm$). Figure 5(b), 5(d) and 5(f) are used to facilitate the understanding of flux distribution. From Fig. 5(a) and Fig. 5(b), it can be seen that $B_{1,r}$ is always normal to the rotor surface. It reaches the maximum value at the center point of PM poles (Point P_2). At points far away from the rotor equator, such as P_1 and P_3, the flux density becomes smaller, but with same positive/negative signs. The flux density at the center of neighboring PM pole (P_4) also has the maximum value, but with opposite sign. In Fig. 5(d), however, $B_{1,\theta}$ should be equal to zero along the rotor equator (P_2, P_4), because the PM poles are symmetrically arranged with respect to the rotor equator. At points on both side of the rotor equator (P_1, P_3), the flux density magnitude increases, but with opposite value. This analysis coincides the variation of $B_{1,\theta}$ in Fig. 5(c). Similarly, in Fig. 5(f), flux density component $B_{1,\phi}$ along the center line of PM pole such as P_1 and P_2 is equal to zero,

because the flux density in ϕ direction is symmetric about the center line. $B_{1,\phi}$ increases at points away from the center line (P_3, P_4), and is relatively larger at point P_4.

B. Effect of Iron Stator on Magnetic Field

Denoting components $5O_{4,6}r^{-6} - 4O_{4,5}r^3$, $O_{4,5}r^3 + O_{4,6}r^{-6}$ and $O_{4,5}r^3 + O_{4,6}r^{-6}$ in Eqns. (35) - (37), as $O_{s,1}$, $O_{s,2}$ and $O_{s,3}$ respectively gives

$$B_{1,r} = \frac{3}{8}\sqrt{\frac{35}{2\pi}}\frac{ac\mu_0 M_0}{\sqrt{\pi}}O_{s,1}\sin^4\theta\cos4\phi \quad (38)$$

$$B_{1,\theta} = \frac{3}{2}\sqrt{\frac{35}{2\pi}}\frac{ac\mu_0 M_0}{\sqrt{\pi}}O_{s,2}\sin^3\theta\cos\theta\cos4\phi \quad (39)$$

$$B_{1,\phi} = \frac{3}{2}\sqrt{\frac{35}{2\pi}}\frac{ac\mu_0 M_0}{\sqrt{\pi}}O_{s,3}\sin^3\theta\sin4\phi \quad (40)$$

The relationship between magnetic flux density components and stator radius can be revealed through the relationships between $O_{s,1}$, $O_{s,2}$, $O_{s,3}$ and stator radius R_s as presented in Fig. 6. From these figures, some conclusions can be obtained.

(a) $B_{1,r}$ (b)

(c) $B_{1,\theta}$ (d)

(e) $B_{1,\phi}$ (f)

Fig. 5. Simulation of magnetic flux density distribution ($r = 46mm$)

1054

- $O_{s,2}$ and $O_{s,3}$ are equal to zero when stator radius is approximately the same as the rotor radius. In other words, the tangential components of flux density $B_{1,\theta}$ and $B_{1,\phi}$ are nearly equal to zero when stator radius approaches the rotor radius.

- $O_{s,1}$ is larger with smaller size of stator radius, which indicates that most fluxes in ϕ and θ directions are "dragged" to r direction due to high permeability of the stator iron. As a result, the flux lines are normal to the stator inner surface when its radius is small.

- The largest value $O_{s,1}$ (when $R_s = 46mm$) is about twice of the smallest one (when R_s is very large). When the stator size is very large, it can be regarded that the stator is made of nonferromagnetic material. Therefore, the magnetic flux density in r direction can be increased about twice by using a iron stator.

- Because the torque output of the spherical actuator is produced by the radial component of magnetic flux density, a stator made of laminated soft iron can help to increase the actuator torque output.
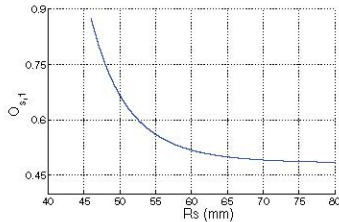
(a) $O_{s,1}$ vs. R_s
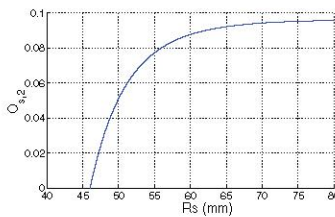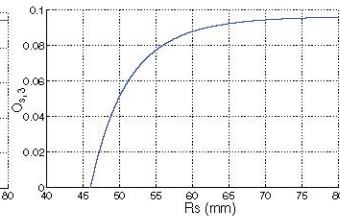
(b) $O_{s,2}$ vs. R_s (c) $O_{s,3}$ vs. R_s

Fig. 6. Relationship between flux density and stator radius ($r = 46$mm)

V. CONCLUSION

This paper studied the magnetic field of a 3-DOF PM spherical actuator with a iron stator. The mathematic model of the magnetic field was derived. The magnetic field distribution was simulated, and the effect of the iron stator on the magnetic field distribution was analyzed. It is found that the employment of laminated iron for the stator fabrication can increase the magnetic field by up to 60%, which may increase the actuator torque output greatly.

ACKNOWLEDGMENT

REFERENCES

[1] F. C. Williams, E. R. Laithwaite, and J. Eastham, "Development and design of spherical induction motors," in *Proceedings of IEE*, Decemeber 1959, pp. 471–847.

[2] E. R. Laithwaite, "Design of spherical motors," *Electrical Times (London)*, vol. 9, pp. 921–925, June 1960.

[3] K. Davey, G. Vachtsevanos, and R. Powers, "The analysis of fields and torques in spherical induction motors," *IEEE Transactions on Magnetics*, vol. 23, no. 1, pp. 273–282, January 1987.

[4] G. J. Vachtevanos, K. Davey, and K. M. Lee, "Development of a novel intelligent robotic manipulator," *IEEE Control Systems Magazine*, vol. 7, no. 3, pp. 9–15, June 1987.

[5] K. M. Lee and C. K. Kwan, "Design concept development of a spherical stepper for robotic applications," *IEEE Transactions on Robotics and Automation*, vol. 7, no. 1, pp. 175–181, February 1991.

[6] K. M. Lee, R. B. Roth, and Z. Zhou, "Dynamic modeling and control of a ball-joint-like variable-reluctance spherical motor," *ASME Journal of Dynamic Systems, Measurement, and Control*, vol. 118, pp. 29–40, March 1996.

[7] J. Wang, G. W. Jewell, and D. Howe, "Analysis, design and control of a novel spherical permanent-magnet actuator," in *IEE Proceedings: Electric Power Applications*, vol. 145, no. 1, January 1998, pp. 61–71.

[8] W. Wang, J. Wang, G. W. Jewell, and D. Howe, "Design and control of a novel spherical permanent magnet actuator with three degrees of freedom," *IEEE/ASME Transactions on Mechatronics*, vol. 8, no. 4, pp. 457–468, December 2003.

[9] J. Wang, G. W. Jewell, and D. Howe, "A novel spherical actuator: design and control," *IEEE Transactions on Magnetics*, vol. 33, no. 5, pp. 4209–4211, September 1997.

[10] ——, "A novel spherical actuator with three degrees-of-freedom," in *IEEE Transactions of Magnetics*, vol. 34, June 1998, pp. 2078–2080.

[11] G. S. Chirikjian and D. Stein, "Kinematic design and commutation of a spherical stepper motor," *IEEE/ASME Transactions on Mechatronics*, vol. 4, no. 4, pp. 342–353, December 1999.

[12] K. Kahlen, I. Voss, C. Priebe, and R. W. De Doncker, "Torque control of a spherical machine with variable pole pitch," *IEEE Transactions on Power Electronics*, vol. 19, no. 6, pp. 1628–1634, November 2004.

[13] K. M. Lee, H. Son, and J. Joni, "Concept development and design of a spherical wheel motor (SWM)," in *Proceedings of the 2005 IEEE/ASME International Conference on Robotics and Automation*, Monterey, California, USA, July 2005, pp. 335–340.

[14] K. M. Lee and H. Son, "Torque model for design and control of a spherical wheel motor," in *Proceedings of the 2005 IEEE/ASME International Conference on Advanced Intelligent Mechatronics*, Monterey, California, USA, July 2005, pp. 335–340.

[15] L. Yan, I. M. Chen, C. K. Lim, G. L. Yang, W. Lin, and K. M. Lee, "Experimental investigation on the magnetic field of a permanent magnet spherical actuator," in *2005 IEEE/ASME International Conference on Advanced Intelligent Mechatronics*, California, USA, July 2005, pp. 341–346.

[16] L. Yan, I. Chen, G. Yang, and K. Lee, "Analytical and experimental investigation on the magnetic field and torque of a permanent magnet spherical actuator," *IEEE/ASME Transactions on Mechatronics*, vol. 11, no. 4, pp. 409–419, August.

[17] L. Yan, I. Chen, C. Lim, G. Yang, W. Lin, and K. Lee, "Design and analysis of a permanent magnet spherical actuator," *IEEE/ASME Transactions on Mechatronics*, p. (accepted), April 2008.

[18] H. Walter, *Introduction to the Principles of Electromagnetism*. USA: Addison-Wesley Publishing Company, Inc., 1971.

[19] J. Wang, W. Wang, and G. W. J. D. Howe, "A novel spherical permanent magnet actuator with three degrees-of-freedom," *IEEE Transactions on Magnetics*, vol. 34, no. 4, pp. 2078–2080, July 1998.

[20] B. Guru and H. Hiziroglu, *Electromagnetic Field Theory Fundamentals*. UK: Cambridge University Press, 2004.

[21] N. O. M. Sadiku, *Elements of Electromagnetics*. USA: Oxford University Press, 2001.